Defect and Diffusion Forum
ISSN: 1662-9507, Vol. 452, pp 45-51
doi:10.4028/p-xjp7QK

Submitted: 2025-09-26
Revised: 2025-12-17
Accepted: 2026-02-23
Online: 2026-05-18

Investigating the Temperature Dependence of Charge Carrier Lifetime in Low-Doped Epitaxial 4H-SiC Layers

Zimo Yuan[1,a], Alex Metreveli[1,b], Lasse Vines[2,c], Orazio Samperi[2,d], Misagh Ghezellou[3,e], Jawad Ul-Hassan[3,f] and Anders Hallén[1,g]

[1]KTH Royal Institute of Technology, SE 164 40 Kista, Sweden

[2]Centre for Material Science and Nanotechnologies, University of Oslo, 0373 Oslo, Norway

[3]Department of Physics, Chemistry and Biology, Linköping University, SE 581 83 Linköping, Sweden

[a]willinf347@gmail.com, [b]alexmet@kth.se, [c]lasse.vines@fys.uio.no, [d]oraziosa@smn.uio.no, [e]misagh.ghezellou@liu.se, [f]jawad.ul-hassan@liu.se, [g]ahallen@kth.se

Keywords: boron, deep levels, SRH recombination, thermodynamics.

Abstract. In this paper, the temperature dependence of charge carrier lifetimes in n-type 4H-SiC epitaxial layers is studied in a temperature range of 300-500 K. It is assumed that shallow (B) and deep (D) boron-related defects are the dominating lifetime killers in as-grown epitaxial layers. The thermodynamic behavior of these two types of defects is obtained from DLTS measurements, and implemented in the Shockley-Read-Hall (SRH) model to calculate lifetimes, using Gibbs free energies to describe the accurate temperature dependence for capture and emission processes of the defects. Calculation results show that the lifetimes controlled by shallow boron defects increase with increasing temperature, while D-defects give the opposite temperature dependence. The theoretical results are also compared to measured data from 10 kV 4H-SiC PiN-structures, showing that the temperature dependence of the effective lifetime can be changed by proton implantations, which gives rise to additional $Z_{1/2}$ defects that have similar temperature effects on lifetimes as D-related defects.

Introduction

Charge carrier lifetime is an important parameter for bipolar 4H-SiC devices, since it has a large impact on device losses and switching speed [1]. It was previously acknowledged that the point defects, especially the carbon vacancies ($Z_{1/2}$ centers), have a dominant effect on controlling lifetimes in 4H-SiC. Recent research, however, has found that the measured lifetimes are not proportional to the abundance of $Z_{1/2}$ at low concentration levels, suggesting that other defects might affect the lifetimes [2]. Boron-related defects [3, 4] in the lower half of the 4H-SiC bandgap have recently been suggested to control the carrier lifetimes at low $Z_{1/2}$ levels from deep level transient spectroscopy (DLTS) analyses, namely the shallow (B) and deep boron (D), respectively. These defects originate from boron contamination incorporated during growth, and can sometimes have higher concentrations than $Z_{1/2}$ [5].

One way to assess the lifetime is by calculations using the Shockley-Read-Hall (SRH) model, in which the bandgap energies, trap concentrations and capture rates of traps are obtained from DLTS measurements. This method also allows the temperature dependence of lifetimes to be determined, but it is also important to use the correct thermodynamic model for the capture and emission processes. This means that the Gibbs free energy, $\Delta G = \Delta H - T\Delta S$, should be used, where H is the enthalpy, T is the absolute temperature and S is the entropy relevant for the carrier transitions [6, 7]. The correct temperature dependence of the carrier lifetime is essential for device modelling, since the 4H-SiC devices operate within a wide temperature range. Although the lifetimes of 4H-SiC devices can be measured experimentally by, for instance, open voltage circuit decay (OCVD) and photoluminescence (PL), there is a need to derive the lifetimes from physical models based on the different recombination centers in the material.

In this work, we extend the SRH model to study the temperature dependence of lifetimes theoretically, assuming that the boron-related defects, the B- and D-defects, are the lifetime killers.

Thermodynamically based properties of these defects are collected from DLTS measurements [2, 8], and are implemented into the SRH model. The results will also be compared to experimental forward IV data of 10 kV 4H-SiC PiN diodes, including also proton implanted devices adding high local concentration of carbon vacancies.

Models

Based on statistics of carrier capture and emission from deep bandgap states, the SRH model is used to calculate the total, effective charge carrier lifetime, τ, summed up over γ different types of defects present in the material [9,10]:

$$\tau^{-1} = \sum_{j=1}^{\gamma} \frac{(n_0 + p_0 + \Delta n) N_{Tj} c_{nj} c_{pj}}{c_{nj}(n_0 + \Delta n + n_j) + c_{pj}(p_0 + \Delta n + p_j)} \tag{1}$$

where n_0 and p_0 are carrier concentrations at thermal equilibrium, Δn is the excess carrier concentration (assuming charge neutrality, $\Delta n = \Delta p$) and N_{Tj} is the concentration of the jth type of defect.

Capture coefficients c_n and c_p can be calculated using the thermal velocity v and capture cross section σ for electrons and holes, respectively:

$$c_{n,p} = \sigma_{n,p} v_{n,p} \tag{2}$$

where the thermal velocities are obtained from the absolute temperature T and the effective masses m_n* and m_p*. The Boltzmann constant is designated by k:

$$v_{n,p} = \sqrt{\frac{3kT}{m^*_{n,p}}} \tag{3}$$

Concentrations n_j and p_j represent the carrier concentrations when the Fermi level is aligned with the energy position of corresponding defects, calculated with Eq. 4 and Eq. 5.

$$n_j = N_C \exp\left(-\frac{E_C - E_{Tj}}{kT}\right) \tag{4}$$

$$p_j = N_V \exp\left(-\frac{E_{Tj} - E_V}{kT}\right) \tag{5}$$

where N_C and N_V are the effective density of states in the conduction band and valence band, and are both temperature dependent. It should also be noted n_j and p_j are now calculated with the traps bandgap positions given by the Gibbs free energies in order to describe the proper thermodynamic behavior of electronic transitions from trap to band edges defects [6,7]. The Gibbs free energy G includes both the enthalpy H and entropy S of the electronic transitions and is given by Eq. (6).

$$\Delta G = \Delta H - T\Delta S \tag{6}$$

Concentrations n_j and p_j are therefore stated as:

$$n_j = N_C \exp\left(-\frac{H_C - H_{Tj}}{kT}\right) \exp\left(\frac{S_C - S_{Tj}}{k}\right) \tag{7}$$

$$p_j = N_V \exp\left(-\frac{H_{Tj} - H_V}{kT}\right) \exp\left(\frac{S_{Tj} - S_V}{k}\right) \tag{8}$$

DLTS measurements offer the possibility to obtain defect parameters that can be implemented into the SRH model to calculate temperature-dependent lifetimes. Following Peaker et al. [11], the activation energy E_a and the apparent capture cross section, σ_a, can be extracted and, through capture

rate measurements, the capture energy barrier E_σ and the true capture cross section σ_∞ can also be obtained.

The enthalpy for the given defect ΔH is calculated by:

$$\Delta H = E_a - E_\sigma \tag{9}$$

The entropy ΔS is calculated by:

$$\Delta S = k \log(\frac{\sigma_a}{\sigma_\infty}) \tag{10}$$

Concentrations n_j and p_j calculated with Gibbs free energies are thus available using Eq. (6), Eq. (9) and Eq. (10).

Results and Discussion

Figure 1 gives a simplified band diagram of 4H-SiC, with the energy positions of three significant traps that are active in the control of charge carrier lifetimes. The double acceptor trap, $Z_{1/2}$, which has been proved to originate from carbon vacancies, is located about 0.67 eV [13] below the bottom of the conduction band. Two boron-related minority traps, shallow B and deep D-center, are closer to the valence band. It has been found that shallow boron, B, and the deep boron, D-center, are assigned to boron impurities occupying the silicon site and carbon site in the SiC lattice, respectively, which leads to completely different energy levels and thermodynamic properties. It should also be noted that associated DLTS peaks (B_1, B_2, D_1 and D_2) from hexagonal and cubic sites [8, 13] are both observed for these two traps, and they will be merged in this work. The energy positions of shallow B and D-centers summarized from the literature are also given in Fig. 1. Table 1 summarizes the recent measured trap parameters [8] that will be used in this work. Since the 4H-SiC lattice contains both hexagonal and cubic sites with slightly varying bandgap positions, and the two versions of the shallow boron, we have used the dominating level in these calculations. In this work, we mainly discuss B- and D-related defects, which correspond to the first and second type of defects in Eq. (1).

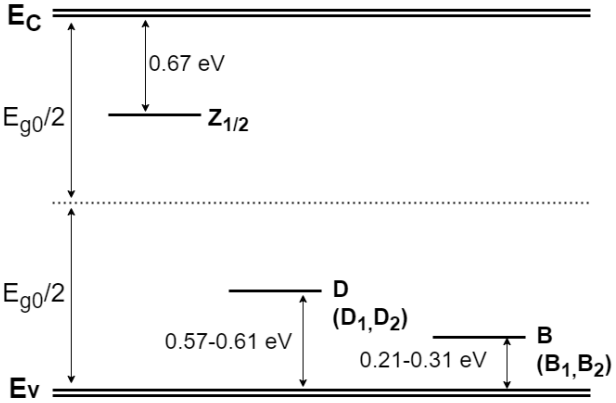

Fig. 1. Three energy levels that are expected to compete for the control of the charge carrier lifetime in low doped 4H-SiC: the majority trap $Z_{1/2}$ and the minority traps shallow B and D-centers. The energy positions of the dominating levels are given in the figure (not in scale).

Table 1. Thermodynamic parameters of shallow B and D-center.

Trap	E_a (eV)	E_σ (eV)	σ_a (cm^2)	σ_∞ (cm^2)
B	0.27	0.10	2.2×10^{-14}	1.87×10^{-14}
D	0.57	0.05	3.93×10^{-14}	1.04×10^{-16}

A 10 kV 4H-SiC PiN diode is used as an example to study the lifetimes in the drift region. The diode has a 120 μm thick drift layer, with a doping concentration of 2×10^{14} cm^{-3}. The SRH lifetimes for shallow B and D-center are computed under high and low injection, with an excess carrier concentration of 3×10^{16} and 1×10^{12} cm^{-3}, respectively. The temperature range is from 298 to 498 K,

covering a substantial part of the operation range of 4H-SiC devices. It should be noted that only the hole capture process of the minority traps has been measured, giving the hole capture cross section σ_p ($\sigma_p = \sigma_a$), enthalpy H_{Tj}-H_V, and entropy S_{Tj}-S_V that can be used to calculate concentration p_j, seen in Eq. (8). The electron transport to these defects has not been measured, and therefore we set $\sigma_n = \sigma_p$ to estimate the electron cross section. The Gibbs free energy term in Eq. (7), G_C-G_{Tj}, is assumed to be $(G_{Tj}$-$G_V)\cdot(E_C$-$E_T)/(E_T$-$E_V)$. These assumptions do not affect the calculations, since the concentration n_j for both B- and D-related defects are negligible within the previously mentioned temperature range.

To start with, we analyze the shallow B level. The term n_1 is negligible due to large G_C-G_{T1}. The term p_1 gives a concentration within the range of 10^{17} cm^{-3}, far more than both Δn and n_0. The approximate high-injection and low-injection SRH lifetime from shallow B, with concentration N_{T1}, are therefore given by Eq. (11) and Eq. (12).

$$\tau_{B(high)} \approx \frac{1}{N_{T1}} \frac{c_{n1} + c_{p1}(1 + \frac{p_1}{\Delta n})}{c_{n1} c_{p1}} \tag{11}$$

$$\tau_{B(low)} \approx \frac{1}{n_0 N_{T1}} \frac{p_1}{c_{n1}} \tag{12}$$

Similarly, for the D-center as the second kind of defects with concentration N_{T2}. With the parameters in Table 1, the term p_2 is now about 10-20% of n_0, meaning that p_2 can also be neglected under a high injection. The corresponding approximate high-injection and low-injection lifetimes are given by Eq. (13) and Eq. (14).

$$\tau_{D(high)} \approx \frac{1}{N_{T2}} \left(\frac{1}{c_{n2}} + \frac{1}{c_{p2}}\right) \tag{13}$$

$$\tau_{D(low)} \approx \frac{1}{n_0 N_{T2}} \frac{c_{n2} n_0 + c_{p2} p_2}{c_{n2} c_{p2}} \tag{14}$$

Note that all the approximate lifetimes from Eq. (11) to Eq. (14) are separated to two terms, one constant term (including n_0 and defect concentrations) and one temperature-dependent term. Figure 2 compares only the temperature-dependent terms for the shallow B and D-center. It can be seen that both the high-injection and low-injection term for shallow B are increasing with temperature, indicating that a higher temperature always increases the shallow B-related SRH lifetime, regardless of the injection level. Meanwhile, an opposite trend can be found for D-center.

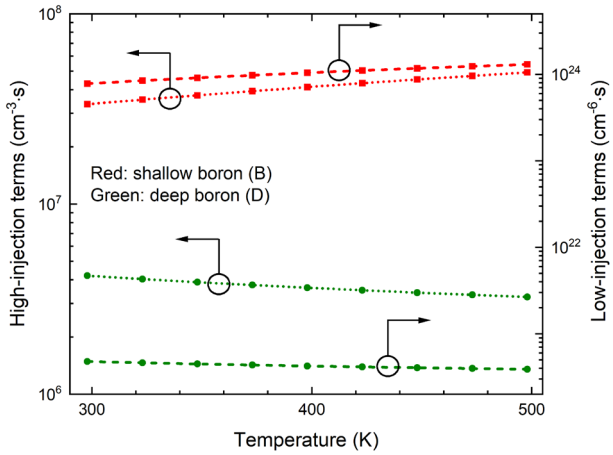

Fig. 2. The temperature dependent part of the SRH lifetimes of shallow B and D-center, at high-injection (Δn=3×10^{16} cm^{-3}) and low-injection (Δn=1×10^{12} cm^{-3}). (Note that the actual lifetime is not plotted, but just the temperature dependent part of equations 11-14, which also leads to different units for high and low injection levels.) Shallow B and D-center related defects have an opposite temperature dependence.

The effective SRH lifetime can now be calculated from Eq. (1). The temperature dependence of the effective lifetime is therefore strongly dependent on which type of trap dominates, i.e. the ratio of concentrations N_{T1} and N_{T2}. Figure 3 shows the calculated high-injection effective lifetimes with different N_{T1}/N_{T2}, where N_{T2} is always set to a constant value (3×10^{12} cm^{-3}). The concentration of B-defects, N_{T1}, has to be at least three times N_{T2} to counteract the temperature dependence of the D-center. A special trend is also observed when N_{T1} is equal to, or slightly higher than N_{T2}, that the effective lifetime first increases and then decreases. The temperature when this happens is between 400 and 500 K.

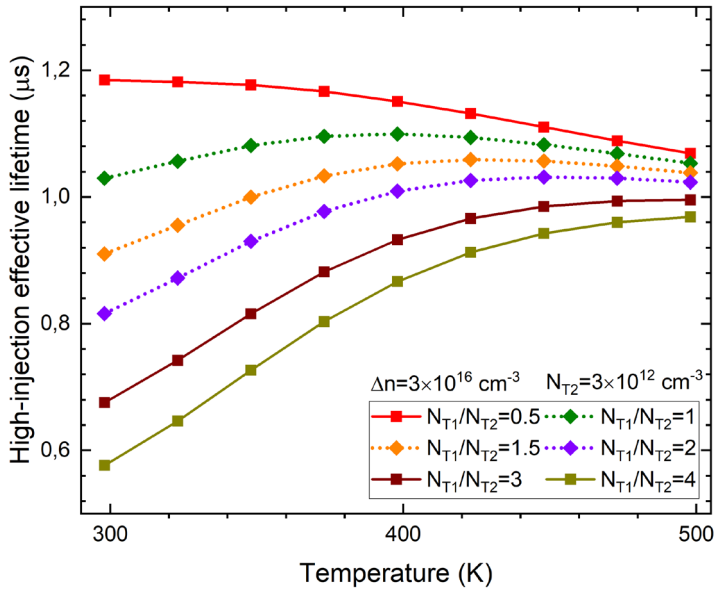

Fig. 3. Calculated effective SRH lifetimes with different concentrations of shallow B-related defects (N_{T1}). The excess carrier concentration is 3×10^{16} cm^{-3}. The effective lifetime decreases with increasing temperature when the D-defects have a higher concentration (N_{T2}) and increases with increasing temperature if B-defects dominate. When the ratio N_{T1}/N_{T2} is between 1 and 2 (dotted lines), the effective lifetime will first increase and then slightly decrease as temperature increases.

Figure 4 shows the lifetime as a function of injection level with the temperature as a parameter. The concentration of the B-defects is much higher (6.7 times) than D-defects, and the same trend described previously can be found when the injection level is higher than 1×10^{16} cm^{-3}. On the low-injection level side, the effective lifetime decreases from 298 to 398 K, and then increases. It can also be found that the low-injection effective lifetime is much higher than high-injection lifetime above 473 K, which is due to the large values of p_j. From fitting measured forward bias IV characteristics with TCAD simulations, it is possible to estimate the change in lifetimes with temperature. The forward IV characteristics of 10 kV PiN diodes [14] used in this work are measured from 298 to 373 K, with a temperature step of 25 K. The diode is also modelled in Sentaurus TCAD.

Figure 5a shows the measured forward IV characteristics (solid lines) of a typical 10 kV diode. The characteristics are shifting to lower voltages, indicating an increase in lifetime with increasing temperature. This is partly due to a reduction of the bandgap at higher temperatures, but the charge carrier lifetimes are also adjusted in the simulations to fit the measured data (dotted lines). For this diode, the drift layer high-injection level lifetimes (the sum of the majority and minority lifetime) used in the simulations are 2.2, 2.6, 3 and 3.5 µs, corresponding to 298, 323, 348 and 373 K. This indicates that B-defect might be the dominant defect in the diode sample.

Figure 5b compares the measured IV characteristics of three samples, two of which have been irradiated with 2.5 MeV protons (dose: 1×10^{9} and 1×10^{10} cm^{-2}) to introduce the intrinsic defect $Z_{1/2}$ in the drift layer with a local peak concentration around 40 µm into the drift layer.

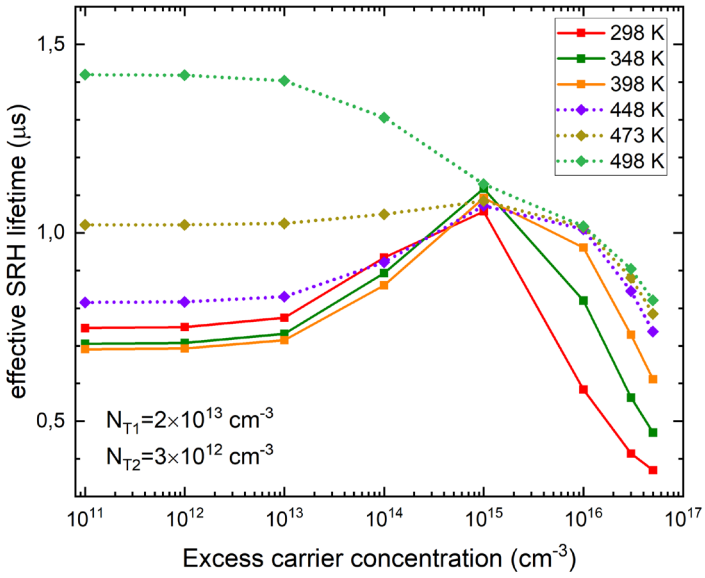

Fig. 4. Calculated effective SRH lifetimes with different temperatures and injection levels. The concentration of B- and D-defects are 2×10^{13} and 3×10^{12} cm^{-3}, respectively. The low-injection effective lifetime rapidly increases when the temperature is over 448 K due to the rapid increase of $p_{1/2}$.

A similar trend of lifetimes as in Fig. 5a is found for the diode irradiated with lower dose, while increasing temperature does not seem to affect lifetimes very much for the sample irradiated with higher dose. A possible explanation for such different temperature effects is the compensation effect of majority traps $Z_{1/2}$ introduced by proton implantation. The activation energy of $Z_{1/2}$ is larger than that of D-center, yielding a similar temperature dependence as the D-center. Proton implantations create a considerable amount of $Z_{1/2}$-related defects, and thus compensate the temperature effects from B-defects.

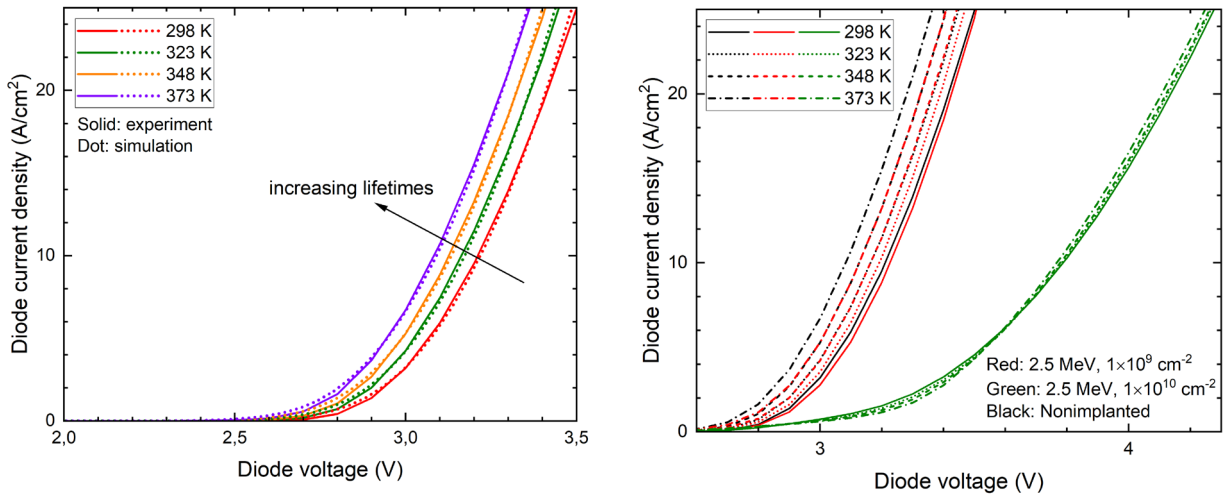

(a) (b)

Fig. 5. (a) Measured and simulated forward IV characteristics of the tested diode from 298 to 373 K. The simulations are used to estimate the lifetimes from the measured characteristics. Experimental results show that increasing temperature increases lifetimes. (b) The measured IV characteristics of diode samples with and without proton implantation (2.5 MeV, 1×10^9 and 1×10^{10} cm^{-2}), giving a strongly non-uniform distribution of defects in the drift layer with a $Z_{1/2}$ peak concentration of 1×10^{14} cm^{-3} [1]. The temperature effects are weaker for the samples treated with proton implantation, possibly due to local compensation of $Z_{1/2}$.

Conclusion

In this work, we have tried to analyze the temperature dependence of charge carrier lifetimes in a lightly-doped n-type 4H-SiC epitaxial layer. It has been assumed that boron-related defects, i.e. shallow B and D-centers, are dominating the lifetimes rather than the $Z_{1/2}$ centers in as-grown epilayers. The parameters of B- and D-related defects are obtained from recent DLTS measurements, and thermodynamic properties are implemented to the SRH model to calculate accurate lifetimes. The calculations show that the temperature dependence of lifetimes controlled by B- and D-related defects are opposite, and the temperature dependence of the total effective lifetime is determined by the defects with a dominant concentration. The results are also compared to measured IV characteristics of devices with varying content of $Z_{1/2}$, and these measurements indicate that MeV proton implantation can counteract the intrinsic temperature dependence of lifetimes in the epitaxial layer by introducing a considerable amount of $Z_{1/2}$ defects.

References

[1] Z. Yuan, et al. "Localized lifetime control of 10 kV 4H-SiC PiN diodes by MeV proton implantation." *Materials Science Forum*. Vol. 1062. Trans Tech Publications Ltd, 2022.

[2] M. Ghezellou, et al. "The role of boron related defects in limiting charge carrier lifetime in 4H–SiC epitaxial layers." *APL Materials* 11.3 (2023).

[3] T. Knezevic, et al. "Boron-Related Defects in N-Type 4H-SiC Schottky Barrier Diodes." *Materials* 16.9 (2023): 3347.

[4] V. J. B. Torres, I. Capan, and J. Coutinho. "Theory of shallow and deep boron defects in 4 H-SiC." *Physical Review B* 106.22 (2022): 224112.

[5] M. E. Bathen, et al. "Impact of carbon injection in 4H-SiC on defect formation and minority carrier lifetime." *Materials Science in Semiconductor Processing* 176 (2024): 108316.

[6] O. Engström and A. Alm. "Thermodynamical analysis of optimal recombination centers in thyristors." *Solid-State Electronics* 21.11-12 (1978): 1571-1576.

[7] P. T. Landsberg, C. Rhys-Roberts and P. Lal. "Auger recombination and impact ionization involving traps in semiconductors."*Proceedings of the Physical Society* 84.6 (1964): 915.

[8] O. Samperi, L. Vines, A. Hallén and M. E. Fragalà, "Charge carrier capture by prominent defect centers in 4H-SiC." Diffusion and Defect Data, Solid State Data. Part A, Defect and Diffusion Forum, ISSN 1012-0386, E-ISSN 1662-9507, Vol. 434, s. 173-182 (2024).

[9] W. Shockley and W. T. Read Jr. “Statistics of the recombination of holes and electrons”. P*hysical Review* 87.5 (1952), p. 835.

[10] R. N. Hall. “Electron-hole recombination in germanium”. *Physical Review* 87.2 (1952), p. 387.

[11] A.R. Peaker, V.P. Markevich, J. Coutinho, "Tutorial: Junction spectroscopy techniques and deep level defects in semiconductors“, *J. Appl. Phys.* 123, 161559 (2018).

[12] N.T. Son, X.T. Trinh, L.S. Lövlie, B.G. Svensson, K. Kawahara, J. Suda, T. Umeda, J. Isoya, T. Makino, T. Oshima, and E. Janzén, „Negative-U System of Carbon Vacancy in 4H-SiC“, Phys. Rev. Lett. 109, 187603 (2012).

[13] M. E. Bathen, et al. "Dual configuration of shallow acceptor levels in 4H-SiC." *Materials Science in Semiconductor Processing* 177 (2024): 08360.

[14] K. Tian, J. Xia, K. Elgammal, A. Schöner, W. Kaplan, R. Karhu, J. Ul-Hassan, A. Hallén“, Modelling the static on-state current voltage characteristics for a 10 kV 4H-SiC PiN diode“, *Materials Science in Semiconductor Processing* 115 (2020): 105097.